Published in final edited form as:
Int J Radiat Oncol Biol Phys. 2013 June 1; 86(2): 292–297. doi:10.1016/j.ijrobp.2013.01.028.

DIFFERENCES IN BRAINSTEM FIBER TRACT RESPONSE TO RADIATION:A LONGITUDINAL DTI STUDY

JINSOO UH, Ph.D.[*], **THOMAS E. MERCHANT, D.O., Ph.D.**[*], **YIMEI LI, Ph.D.**[†], **TIANSHU FENG, M.S.**[†], **AMAR GAJJAR, M.D.**[‡], **ROBERT J. OGG, Ph.D.**[*], and **CHIAHO HUA, Ph.D.**[*]

[*]Department of Radiological Sciences, St. Jude Children's Research Hospital, Memphis, TN, USA

[†]Department of Biostatistics, St. Jude Children's Research Hospital, Memphis, TN, USA

[‡]Department of Oncology, St. Jude Children's Research Hospital, Memphis, TN, USA

Abstract

Purpose—To determine if radiation-induced changes in white matter tracts are uniform across the brainstem.

Methods and Materials—We analyzed serial diffusion tensor imaging (DTI) data, acquired before radiation therapy and over 48-72 months of follow-up, from 42 pediatric patients (age 6-20 years) with medulloblastoma. FSL software (FMRIB, Oxford, UK) was used to calculate fractional anisotropy (FA) and axial, radial, and mean diffusivities. For a consistent identification of volumes of interest, the parametric maps of each patient were transformed to a standard brain space (MNI152), on which we identified volumes of interest including corticospinal tract (CST), medial lemniscus (ML), transverse pontine fiber (TPF), and middle cerebellar peduncle (MCP) at the level of pons. Temporal changes of DTI parameters in VOIs were compared using a linear mixed effect model.

Results—Radiation-induced white matter injury was marked by a decline in FA after treatment. The decline was often accompanied by decreased axial diffusivity and/or increased radial diffusivity. This implied axonal damage and demyelination. We observed that the magnitude of the changes was not always uniform across substructures of the brainstem. Specifically, the changes in DTI parameters for TPF were more pronounced than in other regions ($p<0.001$ for FA) despite similarities in the distribution of dose. We did not find a significant difference among CST, ML, and MCP in these patients ($p>0.093$ for all parameters).

Conclusions—Changes in structural integrity of white matter tracts, assessed by DTI, were not uniform across the brainstem after radiation therapy. These results support a role for tract-based assessment in radiation treatment planning and determination of brainstem tolerance.

Keywords

diffusion tensor imaging (DTI); brainstem; medulloblastoma; white matter injury

Corresponding author: Jinsoo Uh, Ph.D., Department of Radiological Sciences, St. Jude Children's Research Hospital, 262 Danny Thomas Place, Memphis, TN 38105. Tel: (901) 595-6545; Fax: (901) 595-3981; jinsoo.uh@stjude.org.

Parts of this paper have been presented at the 2012 AAPM annual meeting in Charlotte, NC, USA.

Conflicts of Interest Notification: No actual or potential conflicts of interest exist.

INTRODUCTION

Therapy-induced injury to the normal brainstem is a concern for the treatment of common childhood brain tumors. Injury to the brainstem may cause deficits in motor and sensory capabilities and coordination functions, which can compromise the quality of life of long-term survivors.

Current data on brainstem toxicity are limited and based on subjective or categorical scoring methods (1). Because of the lack of tools for assessing sub-structures, the brainstem has often been regarded as a single organ and the dose constraint has been determined without considering the regional sensitivity within the brainstem. Some studies have placed separate limits on the maximum dose to the “center” and “surface” of the brainstem (2), but the rationale for this practice is not clear and no systematic evaluation has been reported.

Diffusion tensor imaging (DTI) is a magnetic resonance imaging (MRI) technique that provides a quantitative assessment of microscopic injuries in the white matter after radiation therapy (3, 4). DTI-derived parameters reflect radiation-induced histologic changes (5) and neurological dysfunctions (6). These findings support the use of DTI as a surrogate marker of brainstem integrity.

Our previous study (7) showed that radiation-induced white matter injury in the brainstem can be detected by DTI-derived parameters. Longitudinal evolution of parameters showed individually distinctive patterns, implying different responses to brainstem injury. In the present work, we extended the previous study, using a larger patient population and longer follow-up times, to investigate whether radiation-induced white matter injury is uniform within the brainstem. Additional sub-structures were analyzed and an extended number of DTI-derived parameters were used. Our previous study included patients with 4 types of brain tumors; the present work included only patients with medulloblastoma in order to minimize variation in the patient group with regard to treatment and statistical group analysis.

METHODS AND MATERIALS

Participants

Between July 2003 and June 2008, 121 pediatric patients diagnosed with CNS embryonal tumors (medulloblastoma, primitive neuroectodermal tumor, or atypical teratoid rhabdoid tumor) were enrolled on a prospective institutional protocol. DTI data were acquired for the patients at postoperative baseline, at the completion of radiation therapy, and every 6 months thereafter up to 72 months. Of the 84 medulloblastoma patients, we selected 42 for the present study, who had follow-up DTI data for more than 48 months (median, 66 months), did not develop necrosis or MRI-proven abnormality in the brainstem, and presented DTI images free from severe artifacts due to metallic dental braces or surgical hardware. Patients younger than 6 years were excluded in this study due to unavailability of age-matched control. The median age at baseline was 10 years (range, 6–20 years).

Another set of DTI data acquired from 52 healthy volunteers (age 6–24 years) was used to distinguish pathological changes in patients from normal age-related changes. Healthy volunteers were enrolled in an institutional functional imaging protocol between October 2007 and April 2011. Two consecutive annual MRI scans were performed on the volunteers.

All protocols were compliant with the Health Insurance Portability and Accountability Act and approved by our institutional review board. Written informed consent and assent were obtained per institutional policy.

Treatment

Patients underwent surgical resection, craniospinal irradiation, and chemotherapy as previously described (7). Risk-adapted radiation therapy was administered, and all patients received adjuvant chemotherapy six weeks after the completion of radiation therapy (see Table 1).

MRI data acquisition

MRI scans on patients were performed on a 1.5T MR scanner (Symphony or Avanto; Siemens Medical Solutions, Enlargen, Germany). DTI data were acquired by a double spin echo pulse sequence, using the following parameters: repetition time = 10,000 ms; echo time = 100 ms; field of view = 230 × 230 mm^2; matrix = 128 × 128; and slice thickness = 3 mm (no gap). Diffusion encoding was applied along either 6 or 12 directions with a diffusion weighting factor (b) of 1000 s/mm^2. One reference image was acquired without the diffusion encoding gradient ($b = 0$ s/mm^2). The DTI scan was repeated 4 times to increase the signal-to-noise ratio. In addition to DTI, a T1-weighted anatomical image with a high resolution (1.25 × 0.82 × 0.82 mm^3) was acquired for the use of spatial registration with computed tomography (CT) and the associated dose distribution. DTI scans on healthy volunteers were performed on a 3T MR scanner (Siemens Tim Trio), in accordance with the functional imaging study protocol. Consequently, a few imaging parameters were different from those of patients: repetition time = 6,500 ms; echo time = 120 ms; field-of-view = 192×192 mm^2; and b-value = 700 s/mm^2. Statistical analysis was designed such that the potential bias in DTI data between the two groups was compensated.

Image processing

A total of 469 DTI data sets were processed from the 42 patients, using FSL (FMRIB, Oxford, UK). All diffusion-weighted images (i.e., with nonzero b-value) were affine-registered to the reference image with a b-value of 0 to remove the effects of patient motion and eddy-current–induced image distortion. Then, the diffusion tensor was estimated for each voxel, from which 4 DTI-derived parameters ("DTI parameters" hereafter for simplicity) were calculated: fractional anisotropy (FA), axial diffusivity (AD), radial diffusivity (RD), and mean diffusivity (MD). For an efficient and consistent regional analysis of the large volume of data, DTI parameter maps were spatially normalized to a standard space (MNI152) by a nonlinear deformation algorithm provided by FSL, so that volumes of interest (VOIs) identified in the standard space could be commonly used for all patient images. Eigenvectors were also normalized via diffusion tensor reorientation (8), and all normalized FA and primary eigenvector images were averaged to generate a standard color-coded FA map (Fig. 1). The CT and the associated dose distribution of each patient were also spatially normalized to the MNI152 space. They were first registered to the T1-weighted image, followed by nonlinear deformation to the standard space.

Volumes of interest

First, the midbrain and pons were delineated on axial images of the standard color-coded FA map (Fig. 1). The midbrain VOI extended in the cranial direction until the thalamus started to appear and to the caudal direction before the transverse pontine fiber (TPF) started to appear. The pons VOI covered axial images showing the TPF. A gap of the DTI slice thickness (3 mm) between the midbrain and pons was not included in the VOIs to avoid the partial volume effect. The corticospinal tract (CST), medial lemniscus (ML), transverse pontine fiber (TPF), and middle cerebellar peduncle (MCP) were further identified at the level of pons. The TPF VOI was separated into 2 compartments: ventral TPF (vTPF) and dorsal TPF (dTPF). It should be noted that the VOIs were named for simplicity and they may include tracts other than the tract referred to by the name; for instance, the ML VOI

may include the spinothalamic tract, the central tegmental tract, or the rubrospinal tract in addition to the medial lemniscus.

Statistical analysis

The mean DTI parameter values at each VOI were calculated, and a statistical analysis was performed to investigate their temporal changes. A mixed effect model was used to analyze the temporal change of the DTI parameter: $DTI = \alpha_0 + \alpha_1 \times age + \alpha_2 \times t \times group + \alpha_3 \times dose + \alpha_4 \times group$. Here, t is the time from the baseline (in year), $group$ is a dummy variable indicating whether the data are from the patient ($group = 1$) or healthy volunteer ($group = 0$), and the Greek letters with subscripts are fitting coefficients. The first two terms model normal age-related change and the following two terms indicate deviation of the patient group from the normal change considering the effect of individual dose differences. The last term, $\alpha_4 \times group$, accounts for potential bias in DTI parameters between the groups at the baseline.

Pairwise comparisons were performed to test whether deviation from the normal pattern in the patient group was the same across different structures. The temporal change from baseline was quantified in terms of the normalized DTI parameter, $nDTI(t) = DTI(t)/DTI(0)$, and the ratio of a pair of VOIs, i and j, was modeled by $nDTI_i(t)/nDTI_j(t) = \beta_0 + \beta_1 \times age_0 + \beta_2 \times t + \beta_3 \times t \times group$. The second term, $\beta_1 \times age_0$, accounts for individual differences in baseline age, age_0. This term was included in the model when it was significant. The estimated coefficient β_3 in the last term indicates how much decline (when $\beta_3 < 0$) or increase (when $\beta_3 > 0$) VOI i shows in the DTI parameter compared with VOI j.

All statistical analyses were performed using the software R (Wirtschaftsuniverstät Wien Vienna University, Austria). A P-value less than 0.05 was considered statistically significant.

RESULTS

Figure 2 shows the average radiation doses in the VOIs over the 42 patients. They were distributed in accordance with proximity to the primary site. The pons was exposed to a higher dose than the midbrain for 39 out of 42 patients. The average doses in the brainstem substructures ranged from 49.4 Gy (vTPF) to 55.4 (ML) and were ordered as follows: vTPF < CST < dTPF < MCP < ML. The differences between any pair of these were statistically significant (paired t-test, $P<0.001$), except for dTPF/MCP and MCP/ML.

DTI parameters showed age-related changes in healthy volunteers. FA increased and RD and MD decreased in all VOIs ($P<0.001$). AD in CST and ML did not show significant changes ($P>0.126$), but decreased in other regions ($P < 0.006$). FA of the patient group negatively deviated from the normal age-related change (i.e., $\alpha_2 < 0$) and was statistically significant in the entire pons, dTPF, vTPF, and MCP ($P < 0.004$). AD and RD also showed negative deviations for all VOIs ($P < 0.034$) except for dTPF and vTPF, where RD deviated positively ($\alpha_2 > 0$, $P < 0.023$). The deviation from the normal pattern was not strongly dependent on individual differences of dose (i.e., $\alpha_3 \times dose$ was not significant) for most VOIs. Only CST showed a significant relation between AD reduction and dose ($\alpha_3 < 0$, $P = 0.03$).

The pairwise comparison between the pons and midbrain showed that the decrease of FA in the pons is more pronounced than that in the midbrain (Fig. 5a). The ratio of the normalized FA between the pons and midbrain showed a negative trend ($\beta_3 = -0.065$, $P < 0.001$). The ratios of the normalized AD and MD also showed significantly negative trends ($P < 0.001$).

Further pairwise comparisons on substructures revealed that the temporal changes of DTI parameters were not uniform within the pons. Figure 3 shows the FA maps of the pons for a patient at baseline and the two follow-up times. The decrease of FA in TPF was manifested at 18 and 45 months from the baseline. In contrast, FA in the CST and ML showed smaller reductions at 18 months and recovered to the baseline level at 45 months. Figure 4 shows comparisons of the temporal changes of the normalized FA of the CST and dTPF for all 42 patients. In most cases, dTPF showed a greater drop than CST and remained at the lower value whereas CST either showed a smaller reduction or eventually recovered to the baseline level.

The statistical analysis confirmed that the ratio of normalized FA between the dTPF and CST showed a significantly negative trend ($\beta_3 = -0.135$, $P < 0.001$, Fig. 5b). The analysis with other DTI parameters was consistent with this result. Taken together, these results suggest that compromised structural integrity is more pronounced in the dTPF than in CST: dTPF showed more significant decrease in AD, increase in RD, and increase in MD than the CST did ($P < 0.001$ for all comparisons, Fig. 5b). Similar results were found when the dTPF was compared to the ML or MCP (Figs. 5c and 5d). On the other hand, no significant differences were observed for the pairs dTPF/vTPF, ML/CST, and MCP/CST in any of the DTI parameters (Figs.5e-5g). In summary, the TPF showed more changes reflecting white matter injury than the CST, ML, and MCP did at the level of pons, regardless of dorsal or ventral compartments, whereas there were no significant differences among the other 3 VOIs.

This regional variation of the temporal changes could not be explained unequivocally by the dose distribution. Although the TPF (either dorsal or ventral) received a smaller dose than the ML (Fig. 2), the TPF showed greater changes than ML (Fig. 5c). We found significant differences between the dTPF and CST (Fig. 5a) but not between the ML and CST (Fig. 5f) or between the MCP and CST (Fig. 5g), which have similar or even greater dose differences. To further investigate the effect of dose on the regional differences in DTI parameter changes, we repeated the pairwise comparison with an additional term, $\beta_4 \times dose_i/dose_j$, in the mixed effect model. Here, $dose_i/dose_j$ is the ratio of dose delivered to VOIs i and j, respectively. We found that this term is not significant ($P > 0.05$) for all pairs of comparisons with all DTI parameters.

DISCUSSION

In this study, we analyzed the temporal changes in DTI parameters measured in the brainstem of patients with medulloblastoma. These changes in patients deviated from the normal age-related changes and suggested white matter injury. This result confirms our previous findings and supports the use of DTI for studying therapy-induced alteration in the brainstem. In addition, we found that the temporal changes in DTI parameters were not always uniform throughout the brainstem.

The normal changes occurring with age in DTI parameters were consistent with previous reports (7, 9). The reduced RD and AD reflect thickening of myelin and increased axonal caliber or number of brain fibers (9). The deviation from the normal pattern for the patient group was prominent in the dTPF and vTPF. The negative and positive deviations of AD and RD in the TPF imply axonal degeneration and demyelination in this structure, respectively. Pairwise comparisons confirmed that the temporal change in the TPF is different from those in other regions.

The differences of DTI parameter changes either across individual patients or different regions were not strongly related to the variation of dose. This is possibly because the dose

was narrowly distributed (see Fig. 2). One consequent implication is that the radiation-induced white matter changes are contributed by factors other than dose. We speculate that the regional intrinsic features of fiber tracts are associated with the response to radiation. However, in order to fully understand tract-specific response to radiation, other clinical factors such as tumor mass, surgical procedure and existing condition also need to be accounted.

Regional sensitivity to radiation therapy has been previously reported. White matter tends to be more sensitive to radiation than gray matter (10) at the same dose level, possibly due to the smaller vascular density of the white matter. For white matter regions, an animal model study showed that the lateral spinal cord is more radiosensitive than the central part in terms of the occurrence of necrosis or hemorrhage (11). Another study on pediatric medulloblastoma patients found more significant changes in FA in the frontal white matter than in the parietal region (12). The pathophysiology of therapy-induced white matter injury has been understood in the context of ischemic effects due to vascular abnormalities or the dysfunction of oligodendrocytes (10, 13). The regional variation of white matter injury has been accordingly explained in terms of the regional differences in vascularity (12) or migration of oligodendrocyte progenitor cells (11). Thus, it would be useful to investigate if that vascularity or oligodendrocyte cell population in the TPF is different from those in other regions.

The TPF is a part of the cortico-ponto-cerebellar tract, which is a major pathway for the motor cortex to communicate with the cerebellum. This tract conveys the information used in the planning and initiation of movement from the cortex to neurons in the pontine gray and subsequently to the cerebellum. White matter injury in TPF may result in symptoms such as ataxia. In the future, we will conduct a correlation study with neurological exams to understand the clinical impact of changes in DTI parameters. It is intriguing that the MCP did not show the structural changes that the TPF did despite these 2 structures belonging to the same fiber tract. The insensitivity of the MCP to radiotherapy has been observed in medulloblastoma and pilocytic astrocytoma patients (14) and has been explained by the extracerebellar localization of the cell bodies of the axons within the MCP.

The dorsal TPF is approximately located in the central area of the pons. Thus, our data partially support the conventional belief that the “center” of the pons is more vulnerable than the “surface.” However, the ventral TPF near the brainstem surface also had a similar response, suggesting that tract-based assessment may provide important insights into determining regional brainstem sensitivity to radiation. This may lead to an adjustment in planning constraints used to minimize brainstem toxicity and associative studies with tract-specific neurological deficits.

The echo-planar imaging in the brainstem region is prone to the effects by magnetic susceptibility differences and pulsation from blood or the cerebrospinal fluid. Recent advances in DTI have allowed high-resolution imaging in localized regions, which is less sensitive to susceptibility variations and motion without compromising the signal-to-noise ratio (15). Such imaging methods would enable the study of additional smaller fiber tracts that were not covered in this work.

In summary, this study showed that radiation-induced white matter changes assessed by DTI were not always uniform within the brainstem. The inspection with the dose distribution suggested that this regional difference may be contributed by factors other than dose. While the clinical impact will be further investigated, we believe this study provides a new insight into planning and evaluation of radiation treatment.

Acknowledgments

Supported in part by the funding from the American Lebanese Syrian Associated Charities and NIH R01 grant HD049888.

References

1. Mayo C, Yorke E, Merchant TE. Radiation associated brainstem injury. Int J Radiat Oncol Biol Phys. 2010; 76:S36–41. [PubMed: 20171516]
2. Debus J, Hug EB, Liebsch NJ, et al. Brainstem tolerance to conformal radiotherapy of skull base tumors. Int J Radiat Oncol Biol Phys. 1997; 39:967–975. [PubMed: 9392533]
3. Khong PL, Kwong DL, Chan GC, et al. Diffusion-tensor imaging for the detection and quantification of treatment-induced white matter injury in children with medulloblastoma: a pilot study. AJNR Am J Neuroradiol. 2003; 24:734–740. [PubMed: 12695214]
4. Nagesh V, Tsien CI, Chenevert TL, et al. Radiation-induced changes in normal-appearing white matter in patients with cerebral tumors: a diffusion tensor imaging study. Int J Radiat Oncol Biol Phys. 2008; 70:1002–1010. [PubMed: 18313524]
5. Wang S, Wu EX, Qiu D, et al. Longitudinal diffusion tensor magnetic resonance imaging study of radiation-induced white matter damage in a rat model. Cancer Res. 2009; 69:1190–1198. [PubMed: 19155304]
6. Chapman CH, Nagesh V, Sundgren PC, et al. Diffusion tensor imaging of normal-appearing white matter as biomarker for radiation-induced late delayed cognitive decline. Int J Radiat Oncol Biol Phys. 2012; 82:2033–2040. [PubMed: 21570218]
7. Hua C, Merchant TE, Gajjar A, et al. Brain tumor therapy-induced changes in normal-appearing brainstem measured with longitudinal diffusion tensor imaging. Int J Radiat Oncol Biol Phys. 2012; 82:2047–2054. [PubMed: 21664060]
8. Alexander DC, Pierpaoli C, Basser PJ, et al. Spatial transformations of diffusion tensor magnetic resonance images. IEEE Transactions on Medical Imaging. 2001; 20:1131–1139. [PubMed: 11700739]
9. Kumar R, Nguyen HD, Macey PM, et al. Regional brain axial and radial diffusivity changes during development. J Neurosci Res. 2012; 90:346–355. [PubMed: 21938736]
10. Schultheiss TE, Kun LE, Ang KK, et al. Radiation response of the central nervous system. Int J Radiat Oncol Biol Phys. 1995; 31:1093–1112. [PubMed: 7677836]
11. Bijl HP, van Luijk P, Coppes RP, et al. Regional differences in radiosensitivity across the rat cervical spinal cord. Int J Radiat Oncol Biol Phys. 2005; 61:543–551. [PubMed: 15667978]
12. Qiu D, Kwong DL, Chan GC, et al. Diffusion tensor magnetic resonance imaging finding of discrepant fractional anisotropy between the frontal and parietal lobes after whole-brain irradiation in childhood medulloblastoma survivors: reflection of regional white matter radiosensitivity? Int J Radiat Oncol Biol Phys. 2007; 69:846–851. [PubMed: 17544593]
13. Calvo W, Hopewell JW, Reinhold HS, et al. Time- and dose-related changes in the white matter of the rat brain after single doses of X rays. Br J Radiol. 1988; 61:1043–1052. [PubMed: 3208008]
14. Rueckriegel SM, Driever PH, Blankenburg F, et al. Differences in supratentorial damage of white matter in pediatric survivors of posterior fossa tumors with and without adjuvant treatment as detected by magnetic resonance diffusion tensor imaging. Int J Radiat Oncol Biol Phys. 2010; 76:859–866. [PubMed: 19540067]
15. Karampinos DC, Van AT, Olivero WC, et al. High-resolution diffusion tensor imaging of the human pons with a reduced field-of-view, multishot, variable-density, spiral acquisition at 3 T. Magn Reson Med. 2009; 62:1007–1016. [PubMed: 19645009]

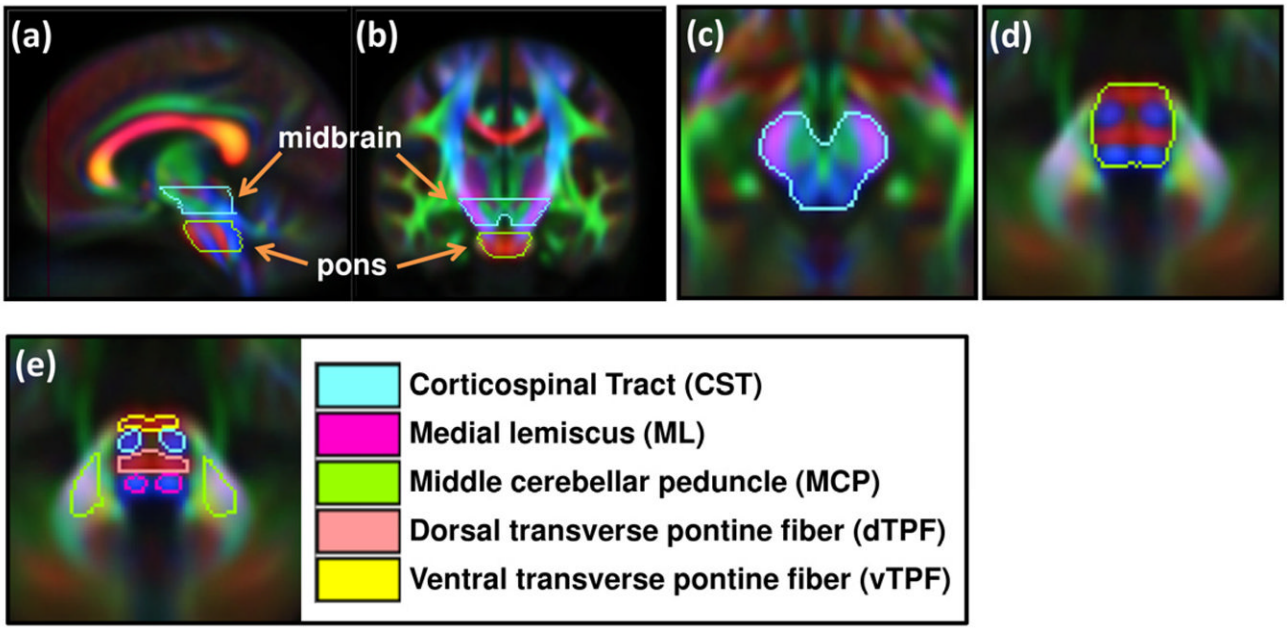

Figure 1.
VOIs drawn on the standard color-coded FA map. (a,b) Sagittal and coronal views of midbrain and pons showing cranial-caudal locations of VOIs. (c,d) Axial views of midbrain and pons. (e) Sub-structures within brainstem.

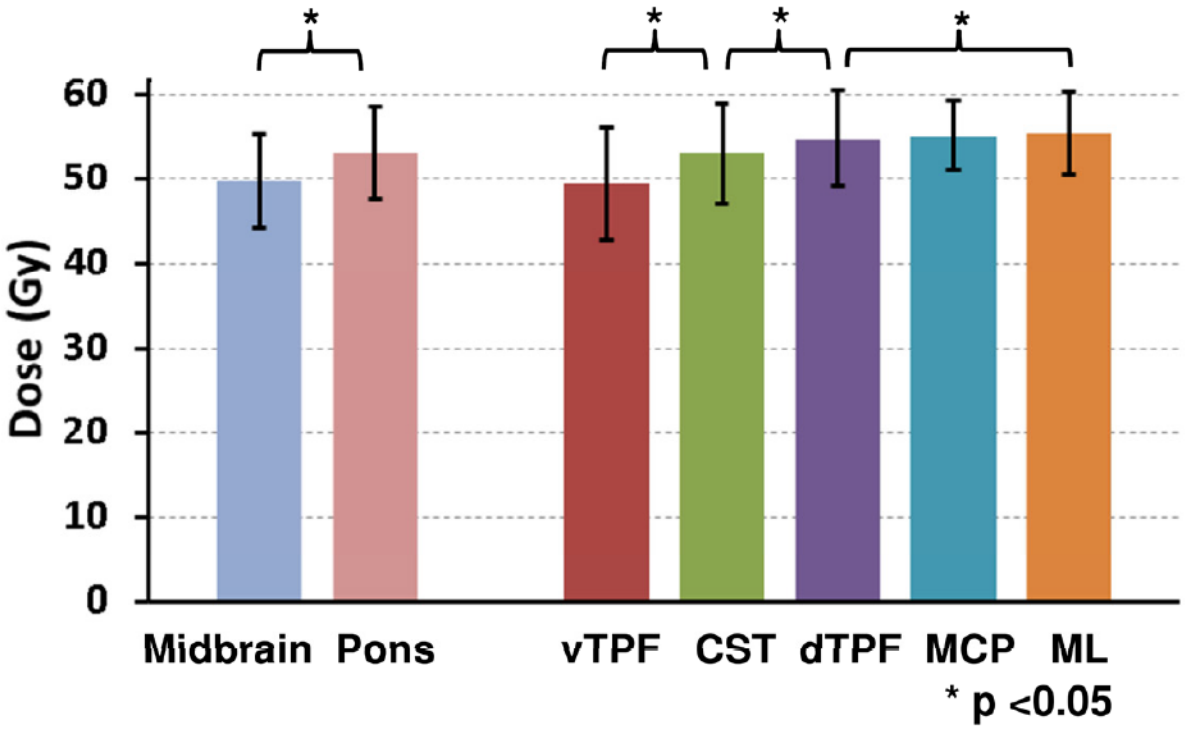

Figure 2.
Average doses in the VOIs over the 42 patients. The error bars indicate standard deviation.

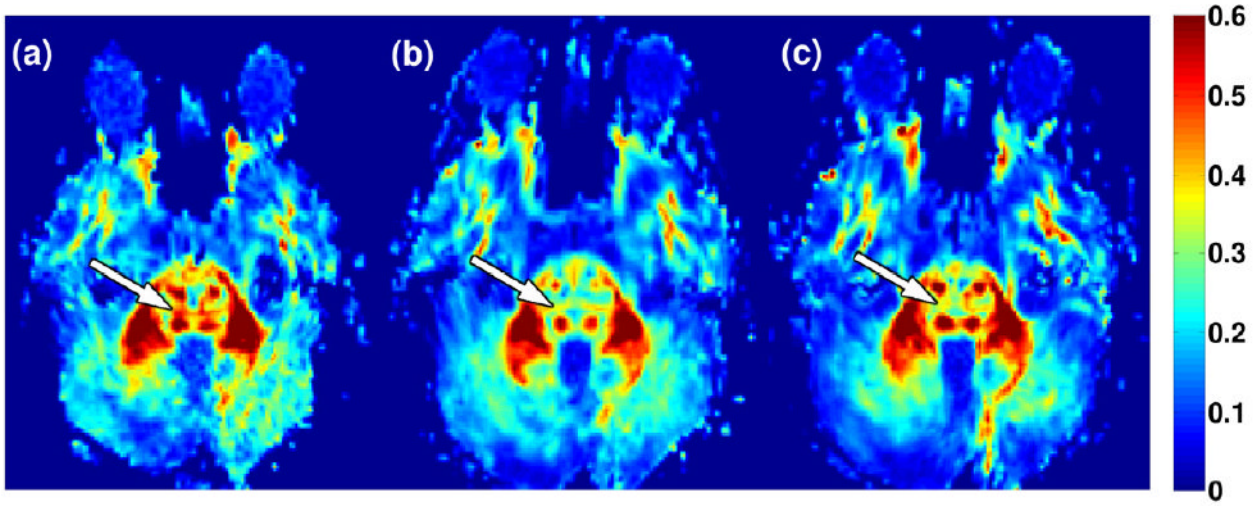

Figure 3.
FA maps of a medulloblastoma patient (male, baseline age 11 years) acquired at baseline (a) and the two follow-up times of 18 months (b) and 45 months (c) from baseline. The white arrows indicate dTPF showing more pronounced FA reduction than the other regions.

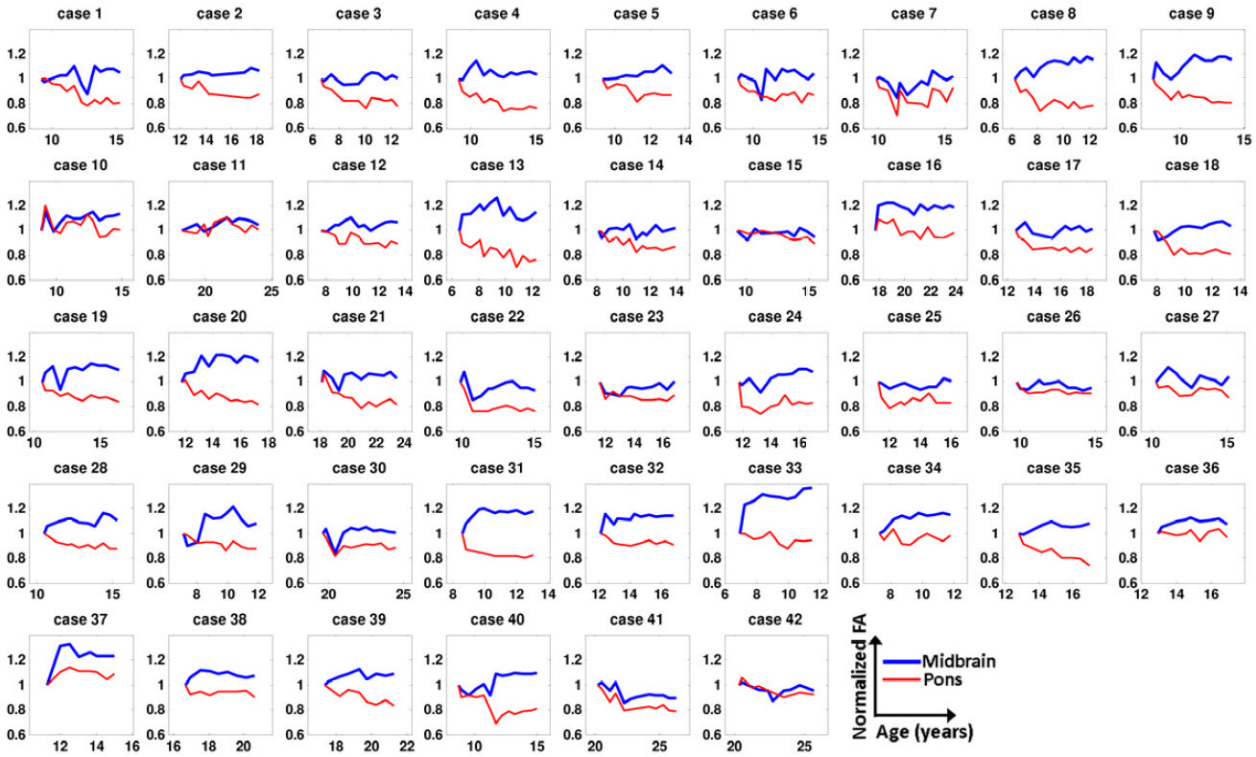

Figure 4.
Temporal plots of FA in CST and dTPF for all 42 patients. Each FA value was normalized by the corresponding baseline value.

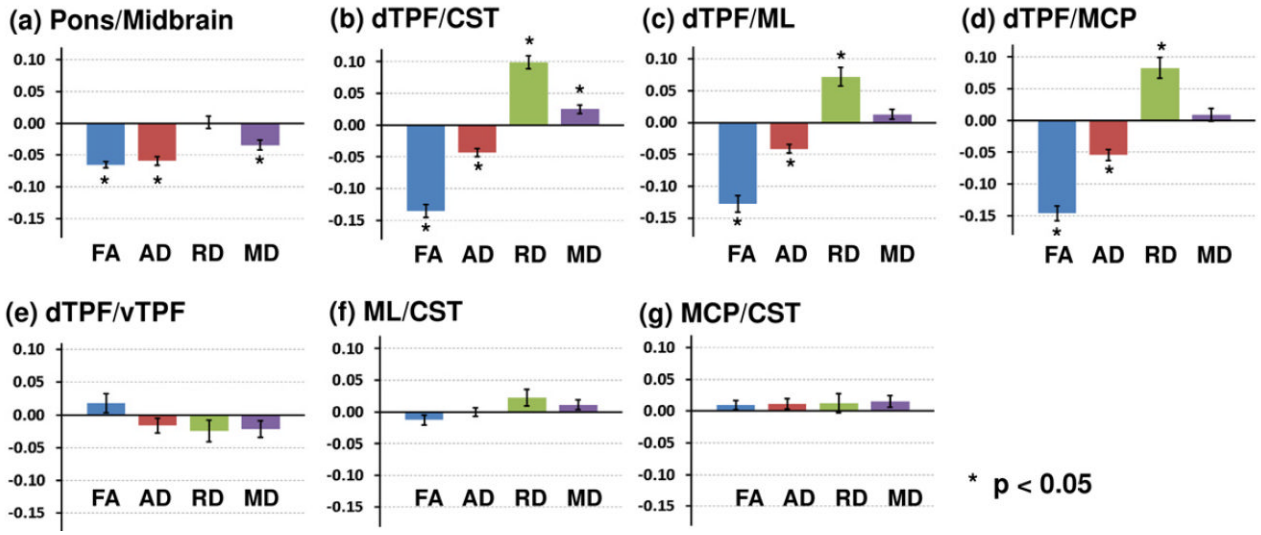

Figure 5.

Pair-wise statistical comparison of the temporal changes of DTI parameters between pairs of VOIs. The number in the ordinate is β_3 in the statistical model equation (see the text) which indicates the temporal change of the VOI in numerator with respect to the one in denominator. The error bars indicate standard error.

Table 1

Characteristics of participants

	Medulloblastoma patients	Healthy volunteers
Total number	42	52
Male	25	31
Female	17	21
Baseline age (years)		
Median	10	12
Range	6 – 20	6 – 24
Risk classification		
Average-risk group	32	–
High-risk group	10	–
Radiation treatment		
Craniospinal irradiation (Gy)	23.4 – 39.6	–
Boost to primary site (Gy)	16.2 – 32.4	–
Total dose to primary site (Gy)	55.8	
Chemotherapy	4 cycles of high-dose cyclophosphamide, cisplatin, and vincristine	–
Extent of resection		–
Gross total resection	37	–
Near total resection (>90%)	5	–